

# Measurements of $\mu \rightarrow 3e$ Decay with Polarised Muons as a Probe of New Physics

P. D. Bolton<sup>a),1</sup> and S. T. Petcov<sup>a,b),2</sup>

<sup>a</sup> *SISSA/INFN, Via Bonomea 265, 34136 Trieste, Italy*

<sup>b</sup> *Kavli IPMU (WPI), UTIAS, The University of Tokyo, Kashiwa, Chiba 277-8583, Japan*

## Abstract

Working within the Standard Model effective field theory approach, we examine the possibility to test charged lepton flavour violating (cLFV) new physics (NP) by angular measurements of the outgoing electron and positrons in the polarised  $\mu^+ \rightarrow e^+e^+e^-$  decay. This decay is planned to be studied with a sensitivity to the branching ratio of  $B_{\mu \rightarrow 3e} \sim 10^{-15}$  by the Mu3e experiment at PSI. To illustrate the potential of these measurements, we consider a set of eight effective operators generating the decay at the tree level, including dimension-five dipole operators and dimension-six scalar and vector four-fermion operators of different chiralities. We show that if the polarised  $\mu^+ \rightarrow e^+e^+e^-$  decay is observed and is induced by a single operator, data from three angular observables – two P-odd asymmetries and one T-odd asymmetry – can allow to discriminate between all considered operators with the exception of scalar and vector operators of opposite chirality. For these two types of operators, the P-odd asymmetry is maximal in magnitude; they can be distinguished, in principle, by measuring the helicities of the outgoing positrons. The observation of a non-zero T-odd asymmetry would indicate the presence in the decay rate of a dipole and vector operator interference term that is T (CP) violating.

---

<sup>1</sup>Email: [patrick.bolton@ts.infn.it](mailto:patrick.bolton@ts.infn.it)

<sup>2</sup>Also at: Institute of Nuclear Research and Nuclear Energy, Bulgarian Academy of Sciences, 1784 Sofia, Bulgaria.

# 1 Introduction

The observation of the charged lepton flavour violating (cLFV) decays  $\mu \rightarrow e\gamma$ ,  $\mu \rightarrow 3e$ ,  $\tau \rightarrow 3\mu$ , etc. and  $\mu - e$  conversion in nuclei, would be a compelling evidence for the existence of new physics (NP) beyond the Standard Model (SM). These processes are forbidden if the individual lepton charges  $L_\ell$ , with  $\ell = e, \mu, \tau$ , are exactly conserved. We know, however, this is not the case from the observation of oscillations between the different flavour neutrinos (antineutrinos)  $\nu_\ell \rightarrow \nu_{\ell'} (\bar{\nu}_\ell \rightarrow \bar{\nu}_{\ell'})$ ,  $\ell \neq \ell'$ ,  $\ell, \ell' = e, \mu, \tau$ , triggered by non-zero neutrino masses and mixing, which imply that  $L_\ell \neq \text{const}$ . This suggests that the cLFV processes should take place at some level. Actually, in any theoretical model of neutrino mass generation that describes correctly the neutrino oscillation data, the cLFV processes would be allowed and, depending on the specific technical aspects of the model, their rates can be predicted to lie within certain ranges. The minimal model of this class is the SM (renormalisable) extension, which includes three  $SU(2)_L$  singlet right-handed (RH) neutrino fields  $\nu_{\ell R}$  whose couplings respect the SM  $SU(2)_L \times U(1)_Y$  gauge symmetry and conserve the total lepton charge  $L = L_e + L_\mu + L_\tau$ . In this case the neutrinos get a Dirac mass term after the spontaneous breaking of the SM symmetry from a Yukawa-type coupling which involves the left-handed (LH) lepton doublets, the Higgs doublet and the RH neutrinos, and the neutrinos with definite mass  $\nu_i$ ,  $i = 1, 2, 3$ , are Dirac particles. Their masses  $m_i$  must satisfy the constraints from existing data: the upper bound on the  $\bar{\nu}_e$  mass,  $m_{\bar{\nu}_e} \simeq m_{1,2,3} < 0.8$  eV [1, 2], and the astrophysical and cosmological upper limits on  $\sum_i m_i$  [3, 4]. The amplitudes of cLFV processes such as  $\mu \rightarrow e\gamma$ ,  $\mu \rightarrow 3e$  and  $\tau \rightarrow 3\mu$  are generated at one-loop level by diagrams involving virtual neutrinos  $\nu_i$  (see, e.g., Ref. [5]). However, the rates of these processes are strongly suppressed by the factor  $m_i^4/M_W^4$  [6], where  $M_W \simeq 80$  GeV is the  $W^\pm$  boson mass, which renders them effectively unobservable. Using the results of Ref. [6] (see also Refs. [7, 8]) and the current neutrino oscillation data, one finds, for example, that the predicted  $\mu \rightarrow e\gamma$  decay branching ratio is  $B_{\mu \rightarrow e\gamma} \simeq 10^{-55}$ , while the current experimental upper bound is  $B_{\mu \rightarrow e\gamma} < 4.2 \times 10^{-13}$  [9].

It is clear, however, that if the neutrino masses in the quoted suppression factor are replaced by, e.g., the masses  $M_j$  of heavy neutral leptons (or heavy Majorana neutrinos)  $N_j$  with values in the range of a few GeV to 1 TeV, the rates of the cLFV processes are enhanced and may be close to the existing upper limits (collected in Table 1) [7, 8, 10, 11]. This is precisely the case (see, e.g., [12–16]) in the low-scale version of the type I seesaw model [17–21], which technically is a straightforward modification of the simple model of neutrino masses and mixing considered above, allowing for the non-conservation of the total lepton charge  $L$  and thus providing a natural explanation of the smallness of the neutrino masses. Via the (low- or high-scale) leptogenesis mechanism, the type I seesaw scenario can also account for the observed baryon asymmetry of the universe and establishes a link between the generation and smallness of the neutrino masses and the origin of the baryon asymmetry.

There are many alternative models of neutrino mass generation (for example, those incorporating a Higgs triplet [22–24], RH fermion triplets [25, 26], radiative neutrino mass generation [27–31] or minimal flavour violation [32–36], etc.) in which the cLFV processes are predicted to have rates close to the existing experimental upper limits (for a review see, e.g., Ref. [37]). Being an important signal for NP, these processes have also been

considered in models with supersymmetry, grand unification and continuous and discrete flavour symmetries [38–46].

Given the quantity and variety of possible NP models in which the cLFV processes are allowed and can proceed with rates close to the existing upper bounds, one can instead study the impact of NP at low energies in the model independent SM effective field theory. Below the scale of NP,  $\Lambda_{\text{NP}}$ , but above the electroweak symmetry breaking (EWSB) scale, one adds higher-dimensional operators to the SM Lagrangian built from SM fields and respecting the  $SU(3)_c \times SU(2)_L \times U(1)_Y$  gauge symmetry,

$$\mathcal{L} = \mathcal{L}_{\text{SM}} + \sum_{d \geq 5} \mathcal{L}^{(d)}; \quad \mathcal{L}^{(d)} = \sum_i \frac{C_i^{(d)}}{\Lambda_{\text{NP}}^{d-4}} \mathcal{O}_i^{(d)}, \quad (1)$$

where  $\mathcal{L}^{(d)}$  contains effective operators  $\mathcal{O}_i^{(d)}$  of mass dimension  $d$  with coefficients  $C_i^{(d)}$ . An operator of dimension  $d$  is suppressed by  $(d - 4)$  powers of  $\Lambda_{\text{NP}}$ . The only operator at dimension-five is the  $|\Delta L| = 2$  Weinberg operator; additional total lepton number violating operators only arise at odd higher dimensions. Lepton flavour can be broken by operators of dimension-five and higher. At energies below the EWSB scale, one must match the above operators onto a set of dimension  $\bar{d}$  operators constructed from light degrees of freedom and respecting the broken-phase  $SU(3)_c \times U(1)_{\text{em}}$  gauge symmetry. The Weinberg and higher-dimensional  $|\Delta L| = 2$  operators, for example, generate Majorana neutrino masses, i.e.  $\mathcal{L}^{(5)} = -\frac{1}{2} M_\nu \bar{\nu}_L^c \nu_L + \text{h.c.}$

Also generated in the low-energy effective field theory are operators which induce cLFV processes. For example, there are 42 (48) operators with three or four legs that trigger the  $\mu \leftrightarrow e$  cLFV processes in Table 1 at tree (one-loop) level [47]. If any of these processes are observed, the question about which operator is generating the process will inevitably arise. The *complementarity* of  $\mu \leftrightarrow e$  cLFV probes in identifying and constraining the possible operators was investigated in Ref. [47–49]. Taken into account was the renormalisation group (RG) running of the operator coefficients from the muon mass  $m_\mu$  up to the electroweak scale,  $M_W$ . It was found that upper bounds on the  $\mu \rightarrow e\gamma$ ,  $\mu \rightarrow e\gamma\gamma$ ,  $\mu \rightarrow 3e$  and  $\mu - e$  conversion in nuclei processes can probe orthogonal directions in the parameter space at a given scale. A higher degree of orthogonality can help discriminate a particular model, in which the indicated processes are triggered by specific combinations of operators whose coefficients at  $\Lambda_{\text{NP}}$  are predicted by the model.

The quoted analyses only used upper limits on the branching ratios and capture rates of  $\mu \leftrightarrow e$  flavour changing processes. If one or more of these processes is detected, additional information can be obtained from the angular distributions and helicities of the final state particles. For example, in Refs. [50], the full differential rate for  $\mu^+ \rightarrow e^+ e^+ e^-$  decay with a *polarised* muon was used to construct three angular distribution asymmetries – two P-odd and one T-odd – sensitive to different combinations of operators (contributing to the process at tree level). The asymmetries were calculated in specific versions of  $SU(5)$  and  $SO(10)$  SUSY grand unified theories and it was found that the sign of the P-odd asymmetry can be different in the two theories.

The consideration of angular observables is particularly relevant as the next generation of  $\mu \leftrightarrow e$  cLFV search experiments are likely to use a polarised muon beam. For example, the high-intensity muon beams (HIMB) proposal at PSI aims to provide a flux of  $\mathcal{O}(10^9)$

cLFV observable	Current upper bound	Future sensitivity
$\mu^+ \rightarrow e^+\gamma$	$4.2 \times 10^{-13}$ [9]	$6 \times 10^{-14}$ [52]
$\mu^+ \rightarrow e^+\gamma\gamma$	$7.2 \times 10^{-11}$ [53]	–
$\mu^+ \rightarrow e^+e^+e^-$	$1.0 \times 10^{-12}$ [54]	$2.0 \times 10^{-15}$ [55]
$\mu^- \mathcal{N} \rightarrow e^- \mathcal{N}$	$7.0 \times 10^{-11}$ (S) [56]	$\sim 10^{-17}$ (Al) [57, 58]
	$4.3 \times 10^{-12}$ (Ti) [59]	$\sim 10^{-18}$ (Ti) [60]
	$7.0 \times 10^{-13}$ (Au) [61]	–
	$4.6 \times 10^{-11}$ (Pb) [62]	–

Table 1: Current upper bounds and future sensitivities on the branching ratios of cLFV muon decays and capture rates for muon to electron conversion in nuclei.

longitudinally polarised muons per second to the Mu3e and MEG II experiments [51], with the average  $\mu^+$  polarisation estimated to be approximately of 93%.

In the present article, following a purely phenomenological approach, we investigate the possibility to discriminate between different effective operators contributing to the amplitude of the polarised  $\mu^+ \rightarrow e^+e^+e^-$  decay by using data on the three angular observables – two P-odd and one T-odd asymmetries. Our aim is not to perform a comprehensive analysis of all operators that can induce the  $\mu^+ \rightarrow e^+e^+e^-$  decay, but to illustrate the potential of the method on the example of a subset of eight commonly used effective operators that generate the decay at tree level. Assuming the scale of NP  $\Lambda_{\text{NP}}$  to be around 1 TeV, one can neglect to a good approximation in the analysed P-odd and T-odd asymmetries the effects of the renormalisation group running of the considered operators above and below the electroweak scale. In addition to the case of having just one operator responsible for the decay, we obtain predictions for the asymmetries of interest also in the cases when two operators are triggering the decay.

This paper is organised as follows. In Section 2, we review the effective operators that are commonly used to parametrise the impact of NP above the EW scale on cLFV observables, such as the  $\mu^+ \rightarrow e^+\gamma$  and  $\mu^+ \rightarrow e^+e^+e^-$  decay rates, and that we are going to use also in our analysis. We then examine the differential branching ratio for the  $\mu^+ \rightarrow e^+e^+e^-$  decay as a function of four kinematic variables, in particular of the two angles defining the directions of the outgoing positrons and electron. We next derive the total branching ratio and single differential branching ratios in the two angles. In doing so, we define three asymmetries (two P-odd and one T-odd) and derive their dependence on the coefficients of the effective operators of interest. We determine further the values of these asymmetries when only one operator, or a combination of two operators, is inducing the decay. In Section 3, we explore how a future experiment such as Mu3e can measure these asymmetries and if so, how the NP contributing to the cLFV process can be identified. We identify some unique signatures and comment on how helicity measurements of the outgoing positrons and electron can complement angular measurements. We conclude in Section 4.

## 2 New Physics Contributions to $\mu^+ \rightarrow e^+e^+e^-$ Decay Rate

In the low-energy effective field theory (LEFT) of the SM, the eight operators of lowest dimension that contribute at tree level to the cLFV  $\mu^+ \rightarrow e^+e^+e^-$  decay rate can be written, without loss of generality (up to Fierz rearrangements), as (see, e.g., [47, 55, 63])

$$\begin{aligned} \mathcal{L}^{(5)} + \mathcal{L}^{(6)} \supset & -2\sqrt{2}G_{\text{F}} \left[ C_{D,L} m_{\mu} \bar{\mu} \sigma_{\alpha\beta} P_L e F^{\alpha\beta} + C_{D,R} m_{\mu} \bar{\mu} \sigma_{\alpha\beta} P_R e F^{\alpha\beta} \right. \\ & + C_{S,LL}^{\ell\ell'} (\bar{\mu} P_L e) (\bar{\ell} P_L \ell') + C_{S,RR}^{\ell\ell'} (\bar{\mu} P_R e) (\bar{\ell} P_R \ell') \\ & + C_{V,LL}^{\ell\ell'} (\bar{\mu} \gamma_{\alpha} P_L e) (\bar{\ell} \gamma^{\alpha} P_L \ell') + C_{V,RR}^{\ell\ell'} (\bar{\mu} \gamma_{\alpha} P_R e) (\bar{\ell} \gamma^{\alpha} P_R \ell') \\ & + C_{V,LR}^{\ell\ell'} (\bar{\mu} \gamma_{\alpha} P_L e) (\bar{\ell} \gamma^{\alpha} P_R \ell') + C_{V,RL}^{\ell\ell'} (\bar{\mu} \gamma_{\alpha} P_R e) (\bar{\ell} \gamma^{\alpha} P_L \ell') \left. \right] \\ & + \text{h.c.} . \end{aligned} \quad (2)$$

Here, the dimension-five operators with coefficients  $C_{D,L}$  and  $C_{D,R}$  are dipole operators and the dimension-six are four-fermion operators. The coefficients have been normalised to the Fermi constant  $G_{\text{F}}$ ; an  $\mathcal{O}(1)$  coefficient therefore corresponds to  $\Lambda_{\text{NP}} \sim m_W$ .

In the presence of the cLFV operators in Eq. (2), the differential branching ratio for  $\mu^+(p) \rightarrow e^+(k_1)e^+(k_2)e^-(k_3)$  decay with an incoming positive muon of polarisation  $\varepsilon = (0, \vec{P})$ , written in the muon rest frame, can be expressed as

$$\begin{aligned} \frac{dB_{\mu \rightarrow 3e}}{dx_1 dx_2 d\Omega_{\varepsilon}} = & \frac{3}{2\pi} \left[ C_1(x_1, x_2) + C_2(x_1, x_2) P \cos \theta_{\varepsilon} \right. \\ & \left. + C_3(x_1, x_2) P \sin \theta_{\varepsilon} \cos \phi_{\varepsilon} + C_4(x_1, x_2) P \sin \theta_{\varepsilon} \sin \phi_{\varepsilon} \right], \end{aligned} \quad (3)$$

where  $d\Omega_{\varepsilon} = d \cos \theta_{\varepsilon} d\phi_{\varepsilon}$ ,  $P = |\vec{P}|$  is the magnitude of the muon polarisation vector, and we define  $x_1 \equiv 2E_{k_1}/m_{\mu}$  and  $x_2 \equiv 2E_{k_2}/m_{\mu}$ , with  $E_{k_1}$  and  $E_{k_2}$  the energies of the outgoing positrons in the muon rest frame (the former taken to have larger outgoing energy,  $E_{k_1} \geq E_{k_2}$ ). For convenience, the  $z$ -axis is set to be along the outgoing electron direction  $\vec{k}_3$  and the decay plane is fixed to be the  $x$ - $z$  plane. The angle  $\theta_{\varepsilon}$  is defined to lie between  $\vec{P}$  and the outgoing electron direction, while the angle  $\phi_{\varepsilon}$  is the azimuthal rotation in the  $x$ - $y$  plane between  $\vec{P}$  and the decay plane. In Eq. (3), the  $C_i(x_1, x_2)$  are functions of the coefficients in Eq. (2) and are given in Appendix A. These expressions are obtained in the limit  $m_e \rightarrow 0$ .

The term in Eq. (6) proportional to  $\cos \theta_{\varepsilon}$  is obtained from the dot product  $k_3 \cdot \varepsilon$ , while the  $\sin \theta_{\varepsilon} \cos \phi_{\varepsilon}$  term originates from the products  $k_1 \cdot \varepsilon$  and  $k_2 \cdot \varepsilon$ . On the other hand, the term proportional to  $\sin \theta_{\varepsilon} \sin \phi_{\varepsilon}$  is generated by  $\varepsilon_{\mu\nu\rho\sigma} \varepsilon^{\mu} k_1^{\nu} k_2^{\rho} k_3^{\sigma}$ , where  $\varepsilon_{\mu\nu\rho\sigma}$  is the four-dimensional Levi-Civita symbol. Under a parity (P) transformation, the polarisation and momentum four-vectors transform as  $\varepsilon \rightarrow \varepsilon' = (0, \vec{P})$  and  $k_i \rightarrow k'_i = (E_{k_i}, -\vec{k}_i)$ , respectively. Under a time (T) reversal, they instead transform as  $\varepsilon \rightarrow \varepsilon' = (0, -\vec{P})$  and  $k_i \rightarrow k'_i = (E_{k_i}, -\vec{k}_i)$ . As a result, the dot products  $k_i \cdot \varepsilon$  and the terms proportional to  $\cos \theta_{\varepsilon}$  and  $\sin \theta_{\varepsilon} \cos \phi_{\varepsilon}$  are P-odd, while  $\varepsilon_{\mu\nu\rho\sigma} \varepsilon^{\mu} k_1^{\nu} k_2^{\rho} k_3^{\sigma}$  and the term proportional to  $\sin \theta_{\varepsilon} \sin \phi_{\varepsilon}$  are T-odd. Assuming that NP contributing to the cLFV process is invariant under CPT, the non-conservation of T implies the violation of CP.

To obtain a double differential branching ratio in the angular variables  $\cos\theta_\varepsilon$  and  $\phi_\varepsilon$ , it is possible to integrate Eq. (3) over the variables  $x_1$  and  $x_2$ . The kinematic limits of the three-body phase space in  $x_1$  and  $x_2$  can be found by first examining those in the kinematic variables  $s_1 = (p-k_1)^2 = m_\mu^2(1-x_1) + m_e^2$  and  $s_2 = (p-k_2)^2 = m_\mu^2(1-x_2) + m_e^2$ . These are

$$4m_e^2 \leq s_1 \leq (m_\mu - m_e)^2, \quad (4)$$

$$s_1 \leq s_2 \leq \frac{1}{2} \left[ m_\mu^2 + 3m_e^2 - s_1 + m_\mu^2 \lambda^{\frac{1}{2}} \left( \frac{m_e^2}{m_\mu^2}, \frac{s_1}{m_\mu^2} \right) \lambda^{\frac{1}{2}} \left( \frac{m_e^2}{s_1}, \frac{m_e^2}{s_1} \right) \right], \quad (5)$$

where  $\lambda(x, y) = (1 - x - y)^2 - 4xy$  and the condition  $s_1 \leq s_2$  follows from  $x_1 \geq x_2$ . Neglecting the electron mass, one obtains the integration ranges  $[0, 1]$  and  $[1 - x_1, x_1]$  for  $x_1$  and  $x_2$ , respectively. However, given the choice  $x_2 \geq x_1$ , one can show that the range  $[0, \frac{1}{2}]$  for  $x_1$  is not physical, so  $[\frac{1}{2}, 1]$  and  $[1 - x_1, x_1]$  can be taken as the final integration limits. These limits lead to logarithmic divergences since the functions  $C_i(x_1, x_2)$ , more specifically, the terms in  $C_i(x_1, x_2)$  proportional to the dipole coefficients  $C_{D,L}$  and  $C_{D,R}$ , which correspond to photon-penguin diagrams, tend to infinity as  $x_1 \rightarrow 1$  (or equivalently, as  $s_1 \rightarrow 0$ ).

In Ref. [50] these collinear singularities were avoided by introducing the cut-off parameter  $\delta$  in the  $x_1$  integration as  $[\frac{1}{2}, 1 - \delta]$ . For all operators in Eq. (3) other than the dipole operators, the  $\delta \rightarrow 0$  limit can be taken without leading to a logarithmic divergence. Non-zero  $\delta$  therefore gives small corrections at higher orders in an expansion in  $\delta$ . On the other hand, the lowest order contribution for the dipole operators is proportional to the logarithm of  $\delta$ . In their numerical estimates, the authors of Ref. [50] fixed  $\delta = 0.02$ . To understand more exactly the dependence on  $m_e$ , we instead perform the phase space integration for the dipole operators over the variables  $s_1$  and  $s_2$ , with the limits in Eqs. (4) and (5) and without neglecting  $m_e$ . This allowed us to avoid introducing an undefined cut-off parameter in the calculations. Finally, we expand the final result in the small ratio  $\hat{m}_e \equiv \frac{m_e}{m_\mu}$ .

We obtain the double differential branching ratio as

$$\frac{dB_{\mu \rightarrow 3e}}{d\Omega_\varepsilon} = \frac{B_{\mu \rightarrow 3e}}{4\pi} \left[ 1 + P(A_{\mu \rightarrow 3e}^P \cos\theta_\varepsilon + A_{\mu \rightarrow 3e}^{P'} \sin\theta_\varepsilon \cos\phi_\varepsilon + A_{\mu \rightarrow 3e}^T \sin\theta_\varepsilon \sin\phi_\varepsilon) \right]. \quad (6)$$

The total branching ratio, which can be found by integrating Eq. (6) over  $\cos\theta_\varepsilon$  and  $\phi_\varepsilon$  with the ranges  $[-1, 1]$  and  $[0, 2\pi]$ , respectively, can be written as

$$B_{\mu \rightarrow 3e} = \frac{1}{8} |C_{S,LL}^{ee}|^2 + 2|C_{V,LL}^{ee}|^2 + |C_{V,LR}^{ee}|^2 - \frac{8}{3} |eC_{D,L}|^2 L_1(\hat{m}_e^2) + 8 \operatorname{Re}[eC_{D,L}(2C_{V,LL}^{ee*} + C_{V,LR}^{ee*})] + (L \leftrightarrow R), \quad (7)$$

where  $L_1(x) = 17 + 12 \ln 4x$ .

Firstly, we note that the terms in the total branching ratio proportional to  $|C_{D,L}|^2$  and  $|C_{D,R}|^2$  are practically equal to previous results in the literature, c.f. Refs [11–13, 41]. Taking only the contribution from  $C_{D,L(R)}$ , we obtain

$$\frac{B_{\mu \rightarrow 3e}^{D,L(R)}}{B_{\mu \rightarrow e\gamma}^{D,L(R)}} = -\frac{e^2}{12\pi} \left( \ln(4\hat{m}_e^2) + \frac{17}{12} \right) \approx \frac{\alpha}{3\pi} \left( \ln \left( \frac{m_\mu^2}{m_e^2} \right) - \frac{11}{4} \right), \quad (8)$$

$C_i^{(\bar{5})}/C_i^{(\bar{6})}$	[50]	[47]	$A_{\mu \rightarrow 3e}^P$	$A_{\mu \rightarrow 3e}^{P'}$
$C_{D,L(R)}$	$A_{R(L)}$	$C_{D,R(L)}$	$\pm 1 \pm \frac{9(17-19 \ln 2)}{17+12 \ln(4\hat{m}_e^2)} \approx \pm 0.63$	$\frac{\pm 144}{5(17+12 \ln(4\hat{m}_e^2))} \approx \mp 0.31$
$C_{S,LL(RR)}^{ee}$	$g_{1(2)}$	$C_{S,RR(LL)}^{ee}$	$\pm 1$	0
$C_{V,LL(RR)}^{ee}$	$g_{4(3)}$	$C_{V,LL(RR)}^{ee}$	$\mp 1$	0
$C_{V,LR(RL)}^{ee}$	$g_{6(5)}$	$C_{V,LR(RL)}^{ee}$	$\pm \frac{1}{3}$	$\pm \frac{32}{105}$

Table 2: Values of the asymmetries  $A_{\mu \rightarrow 3e}^P$  and  $A_{\mu \rightarrow 3e}^{P'}$  when each of the coefficients of the operators in Eq. (2) are taken to be non-zero at a time, with the equivalent coefficients of Refs. [47, 50] shown for clarity.

where we have used the result  $B_{\mu \rightarrow e\gamma} = 384\pi^2(|C_{D,L}|^2 + |C_{D,R}|^2)$ .

The differential branching ratio in  $\cos \theta_\varepsilon$  can be found by integrating Eq. (6) over the azimuthal angle. This gives

$$\frac{dB_{\mu \rightarrow 3e}}{d \cos \theta_\varepsilon} = \frac{B_{\mu \rightarrow 3e}}{2} (1 + A_{\mu \rightarrow 3e}^P P \cos \theta_\varepsilon). \quad (9)$$

The P-odd asymmetry term  $A_{\mu \rightarrow 3e}^P$  that remains is

$$A_{\mu \rightarrow 3e}^P = \frac{1}{B_{\mu \rightarrow 3e}} \left[ \frac{1}{8} |C_{S,LL}^{ee}|^2 - 2 |C_{V,LL}^{ee}|^2 + \frac{1}{3} |C_{V,LR}^{ee}|^2 - \frac{8}{3} |e C_{D,L}|^2 L_2(\hat{m}_e^2) \right. \\ \left. - 8 \operatorname{Re} [e C_{D,L} (2 C_{V,LL}^{ee*} - C_{V,LR}^{ee*})] - (L \leftrightarrow R) \right], \quad (10)$$

where  $L_2(x) = 170 - 171 \ln 2 + 12 \ln 4x$ . In Table 2, we show the values of the asymmetry  $A_{\mu \rightarrow 3e}^P$  when each of the coefficients in Eq. (2) is taken to be non-zero at a time. The operators with coefficients  $C_{S,LL}^{ee}$ ,  $C_{S,RR}^{ee}$ ,  $C_{V,LL}^{ee}$  and  $C_{V,RR}^{ee}$  induce maximal asymmetries,  $A_{\mu \rightarrow 3e}^P = \pm 1$ , while those with coefficients  $C_{D,L}$ ,  $C_{D,R}$ ,  $C_{V,LR}^{ee}$  and  $C_{V,RL}^{ee}$  have  $|A_{\mu \rightarrow 3e}^P| < 1$ . As is evident from Eq. (10), the value of  $A_{\mu \rightarrow 3e}^P$  changes sign when the replacement  $L \leftrightarrow R$  is made. We note that the only operators that interfere at lowest order in  $\hat{m}_e$ , among those considered by us, are the dipole and vector operators. Interference between other operators can therefore be neglected.

One can obtain the differential branching ratio in the azimuthal angle  $\phi_\varepsilon$  by integrating Eq. (6) over  $\cos \theta_\varepsilon$ , giving

$$\frac{dB_{\mu \rightarrow 3e}}{d\phi_\varepsilon} = \frac{B_{\mu \rightarrow 3e}}{2\pi} \left[ 1 + \frac{\pi}{4} P (A_{\mu \rightarrow 3e}^{P'} \cos \phi_\varepsilon + A_{\mu \rightarrow 3e}^T \sin \phi_\varepsilon) \right] \quad (11)$$

$$\equiv \frac{B_{\mu \rightarrow 3e}}{2\pi} \left[ 1 + A_{\mu \rightarrow 3e}^{P'T} P \cos(\phi_\varepsilon + \omega_{\mu \rightarrow 3e}^{P'T}) \right], \quad (12)$$

with  $A_{\mu \rightarrow 3e}^{P'T} = \frac{\pi}{4} \operatorname{sgn}(A_{\mu \rightarrow 3e}^{P'}) \sqrt{(A_{\mu \rightarrow 3e}^{P'})^2 + (A_{\mu \rightarrow 3e}^T)^2}$  and  $\omega_{\mu \rightarrow 3e}^{P'T} = \tan^{-1}(-A_{\mu \rightarrow 3e}^T/A_{\mu \rightarrow 3e}^{P'})$ .

Here, the P-odd asymmetry  $A_{\mu \rightarrow 3e}^{P'}$  is given by

$$A_{\mu \rightarrow 3e}^{P'} = \frac{1}{B_{\mu \rightarrow 3e}} \frac{128}{35} \left[ \frac{1}{12} |C_{V,LR}^{ee}|^2 - 21 |eC_{D,L}|^2 + \text{Re}[eC_{D,L}(3C_{V,LL}^{ee*} - 2C_{V,LR}^{ee*})] - (L \leftrightarrow R) \right], \quad (13)$$

and the T-odd asymmetry  $A_{\mu \rightarrow 3e}^T$  by

$$A_{\mu \rightarrow 3e}^T = \frac{1}{B_{\mu \rightarrow 3e}} \frac{128}{35} \left[ -\text{Im}[eC_{D,L}(3C_{V,LL}^{ee*} - 2C_{V,LR}^{ee*})] + (L \leftrightarrow R) \right]. \quad (14)$$

Fewer operators in Eq. (2) contribute to these asymmetries at leading order in  $m_e/m_\mu$ . In Table 2, we show the values of the asymmetry  $A_{\mu \rightarrow 3e}^{P'}$  when each of the coefficients in Eq. (2) is taken to be non-zero at a time. In isolation, the scalar and vector operators with coefficients  $C_{S,LL}^{ee}$ ,  $C_{S,RR}^{ee}$ ,  $C_{V,LL}^{ee}$  and  $C_{V,RR}^{ee}$  do not contribute to either  $A_{\mu \rightarrow 3e}^{P'}$  or  $A_{\mu \rightarrow 3e}^T$ , while only the imaginary part of the interference between dipole and vector operators contributes to  $A_{\mu \rightarrow 3e}^T$ .

The general expressions for the three asymmetries are compatible with those derived in Ref. [50]. In contrast, our asymmetry  $A_{\mu \rightarrow 3e}^P$  does not depend on the cut-off parameter  $\delta$  which was set to  $\delta = 0.02$  in the numerical estimates in [50]. In our case, the role of this parameter is played by  $4m_e^2/m_\mu^2$ . In addition, the expressions for our asymmetries are a factor of two larger than those reported in Ref. [50] as a consequence of the way we define them. Further, our T-odd asymmetry is of opposite sign.

In order to observe CP violation in the  $\mu^+ \rightarrow e^+e^+e^-$  decay, both the dipole and vector operators must be present; additionally, the coefficients of these operators must have a non-zero relative phase. This is possible, for example, in the canonical type I seesaw [12–14] and general SUSY [64,65] extensions. In the former, the dipole coefficient  $C_{D,L}$  is generated by a photon-penguin diagram with a heavy neutral lepton and  $W^\pm$  boson in the loop. The vector coefficient  $C_{V,LL}^{ee}$ , on the other hand, gets contributions from box diagrams containing two heavy neutral leptons and  $W^\pm$  bosons. The penguin and box diagram amplitudes are proportional to  $U_{ei}U_{\mu j}^*$  and  $U_{ei}U_{\mu j}^*U_{ei}U_{ej}^*$ , respectively, where  $U_{\ell i}$  is the mixing between the charged lepton  $\ell$  and neutrino mass eigenstate  $N_i$  ( $i = 1, \dots, 3+n$ , with  $n$  the number of heavy neutral leptons). The dependence of the coefficients  $C_{D,L}$  and  $C_{V,LL}^{ee}$  on additional Dirac CP phases in the extended mixing matrix can therefore be different. In SUSY extensions, the coefficients can also depend differently on phases in the soft SUSY-breaking sector.

### 3 Phenomenological Analysis

We next discuss the implications of a detection of the  $\mu^+ \rightarrow e^+e^+e^-$  decay of a polarised  $\mu^+$ . We consider, in particular, how angular and spin measurements of the outgoing positrons and electron can help to identify the NP contributing to the cLFV process.

In future, the  $\mu^+ \rightarrow e^+e^+e^-$  decay will be searched for by the Mu3e experiment at PSI. Phase I of the experiment will receive  $\mathcal{O}(10^8)$  positive muons per second with average

momenta  $p \sim 29.8$  MeV from pion decays at rest near the surface of the production target (the  $\pi$ E5 compact muon beamline). The muons produced in this way are fully polarised; the beam is thus estimated to have an average polarisation of  $P \sim 93\%$ . This phase of the experiment is expected to probe down to  $B_{\mu \rightarrow 3e} \sim 2 \times 10^{-15}$ , in contrast to the current limit of  $B_{\mu \rightarrow 3e} < 1.0 \times 10^{-12}$  from the SINDRUM experiment [54]. This is a much larger improvement on the current experimental bound compared to that expected with the planned search for the  $\mu^+ \rightarrow e^+ \gamma$  process. Using the  $\pi$ E5 beamline, the MEG II experiment aims to reach  $B_{\mu \rightarrow e \gamma} \sim 6 \times 10^{-14}$  compared the current bound of  $B_{\mu \rightarrow e \gamma} < 4.2 \times 10^{-13}$  from the original MEG experiment. In the longer term, the HIMB proposal aims to provide  $\mathcal{O}(10^9)$  muons per second to Phase II of the Mu3e experiment, allowing to reach even higher sensitivity to  $B_{\mu \rightarrow 3e}$ . The Mu3e detector is designed to optimally track the positrons and electron from decays of muons at rest, and therefore to fully reconstruct the event kinematics. To cover a large portion of the final-state phase space, the experiment aims to reconstruct tracks over a large solid angle (limited by the beam entry and exit points) with momenta ranging from  $\sim 1$  MeV to half the muon mass [55]. The experiment must be able to discriminate the  $\mu^+ \rightarrow e^+ e^+ e^-$  decay from backgrounds such as  $\mu^+ \rightarrow e^+ e^+ e^- \nu \bar{\nu}$  and a Michel positron accompanied by a  $e^+ e^-$  pair from photon conversion or Bhabha scattering. The experiment can nevertheless exploit the kinematics of the  $\mu^+ \rightarrow e^+ e^+ e^-$  decay at rest,  $|\sum_i \vec{k}_i| = 0$  and  $\sum_i E_{k_i} = m_\mu$ , to mitigate these backgrounds.

To understand how the asymmetries can be measured by an experiment such as Mu3e (in the scenario where  $\mu^+ \rightarrow e^+ e^+ e^-$  is observed), we note that they can be extracted from Eq. (6) as follows:

$$A_{\mu \rightarrow 3e}^P = \frac{2}{P} \int_0^{2\pi} d\phi_\varepsilon \left( \int_0^1 - \int_{-1}^0 \right) d \cos \theta_\varepsilon \frac{1}{B_{\mu \rightarrow 3e}} \frac{dB_{\mu \rightarrow 3e}}{d\Omega_\varepsilon}, \quad (15)$$

$$A_{\mu \rightarrow 3e}^{P'} = \frac{2}{P} \left( \int_{-\frac{\pi}{2}}^{\frac{\pi}{2}} - \int_{\frac{\pi}{2}}^{\frac{3\pi}{2}} \right) d\phi_\varepsilon \int_{-1}^1 d \cos \theta_\varepsilon \frac{1}{B_{\mu \rightarrow 3e}} \frac{dB_{\mu \rightarrow 3e}}{d\Omega_\varepsilon}, \quad (16)$$

$$A_{\mu \rightarrow 3e}^T = \frac{2}{P} \left( \int_0^\pi - \int_{-\pi}^0 \right) d\phi_\varepsilon \int_{-1}^1 d \cos \theta_\varepsilon \frac{1}{B_{\mu \rightarrow 3e}} \frac{dB_{\mu \rightarrow 3e}}{d\Omega_\varepsilon}. \quad (17)$$

The P-odd asymmetry  $A_{\mu \rightarrow 3e}^P$  can be determined by counting the number of electrons with outgoing angles  $\theta_\varepsilon$  in the range  $[0, \frac{\pi}{2}]$  minus those in the range  $[\frac{\pi}{2}, \pi]$ . Other than the outgoing electron direction, this only requires knowledge of the magnitude and direction of the muon polarisation  $\vec{P}$ . To instead determine the P-odd and T-odd asymmetries  $A_{\mu \rightarrow 3e}^{P'}$  and  $A_{\mu \rightarrow 3e}^T$ , it is also necessary to measure the directions of the outgoing positrons to identify the decay plane and the azimuthal angle  $\phi_\varepsilon$ . The asymmetry  $A_{\mu \rightarrow 3e}^{P'}$  can be ascertained by counting the number of decay topologies with angles  $\phi_\varepsilon$  in the range  $[-\frac{\pi}{2}, \frac{\pi}{2}]$  minus those in the range  $[\frac{\pi}{2}, \frac{3\pi}{2}]$ . Conversely, for the asymmetry  $A_{\mu \rightarrow 3e}^T$  one counts the number of decays with angles  $\phi_\varepsilon$  in the range  $[0, \pi]$  minus those in the range  $[-\pi, 0]$ .

In Table 2 we have already shown the values of the asymmetries  $A_{\mu \rightarrow 3e}^P$  and  $A_{\mu \rightarrow 3e}^{P'}$  when each effective coefficient is taken to be non-zero at a time. It follows from the results in Table 2 that the measurement of  $A_{\mu \rightarrow 3e}^P$  can allow to discriminate between the dipole, scalar  $RR$  (scalar  $LL$ ), vector  $LL$  (vector  $RR$ ), vector  $LR$  and vector  $RL$  operators, while it will be impossible to distinguish between scalar  $RR$  (scalar  $LL$ ) and vector  $RR$  (vector

$C_i^{(\bar{5})}/C_i^{(\bar{6})}$	Final-state helicities
$C_{D,L(R)}$	$\mu^+ \rightarrow e_{R(L)}^+ e_{R/L}^+ e_{L/R}^-$
$C_{S,LL(RR)}^{ee}$	$\mu^+ \rightarrow e_{R(L)}^+ e_{R(L)}^+ e_{R(L)}^-$
$C_{V,LL(RR)}^{ee}$	$\mu^+ \rightarrow e_{R(L)}^+ e_{R(L)}^+ e_{L(R)}^-$
$C_{V,LR(RL)}^{ee}$	$\mu^+ \rightarrow e_{R(L)}^+ e_{L(R)}^+ e_{R(L)}^-$

Table 3: Helicities of the outgoing positrons and electron when the  $\mu^+ \rightarrow e^+ e^+ e^-$  decay is induced by each of the operators in Eq. (2).

$LL$ ) operators. With the measurement of  $A_{\mu \rightarrow 3e}^{P'}$  alone it may be possible to discriminate between the dipole, scalar or vector  $LL$  or  $RR$ , and vector  $LR$  or  $RL$  operators. At the same time, the difference between the values of  $A_{\mu \rightarrow 3e}^{P'}$  due to the dipole  $R$  (dipole  $L$ ) and vector  $RL$  (vector  $LR$ ) operators is very small and thus distinguishing between these operators requires an extremely high precision in the measurement of  $A_{\mu \rightarrow 3e}^{P'}$ .

If more than one operator is present, the asymmetries instead take a range of values depending on the relative sizes of the respective coefficients. For example, in the presence of the vector coefficients  $C_{V,LL}^{ee}$  and  $C_{V,LR}^{ee}$  (with all other coefficients set to zero), we have

$$A_{\mu \rightarrow 3e}^P = -1 + \frac{4}{3(1+2x)}, \quad A_{\mu \rightarrow 3e}^{P'} = \frac{32}{105(1+2x)}; \quad x \equiv \frac{|C_{V,LL}^{ee}|^2}{|C_{V,LR}^{ee}|^2}, \quad (18)$$

which clearly range from the minimum values  $A_{\mu \rightarrow 3e}^P = -1$  and  $A_{\mu \rightarrow 3e}^{P'} = 0$  when  $x \gg 1$  and the maximum values  $A_{\mu \rightarrow 3e}^P = \frac{1}{3}$  and  $A_{\mu \rightarrow 3e}^{P'} = \frac{32}{105}$  when  $x \ll 1$ . Actually, the values of the asymmetries  $A_{\mu \rightarrow 3e}^P$  and  $A_{\mu \rightarrow 3e}^{P'}$  are correlated:  $A_{\mu \rightarrow 3e}^{P'} = \frac{8}{35}(1 + A_{\mu \rightarrow 3e}^P)$ . An experimental observation of this correlation would be strong evidence that a combination of the vector  $LL$  and  $LR$  operators are triggering the  $\mu^+ \rightarrow e^+ e^+ e^-$  decay.

A measurement of the maximal asymmetry  $A_{\mu \rightarrow 3e}^P = 1$  ( $-1$ ) would imply that one of the coefficients  $C_{S,LL}^{ee}$  or  $C_{V,RR}^{ee}$  ( $C_{S,RR}^{ee}$  or  $C_{V,LL}^{ee}$ ) dominates over the others. The other P-odd asymmetry  $A_{\mu \rightarrow 3e}^{P'}$  is approximately zero when both  $C_{S,LL}^{ee}$  and  $C_{V,RR}^{ee}$  dominate, while the T-odd asymmetry (which relies on the interference between the dipole and vector operators) is also suppressed; neither can therefore be used to discriminate the two contributions. However, the scalar and vector operators can be distinguished with an additional measurement of the helicity of the outgoing positrons. In Table 3, we show the helicities of the final states for each of the operators in Eq. (2). For both the scalar and vector operators (with the coefficients  $C_{S,LL}^{ee}$  and  $C_{V,RR}^{ee}$ , respectively) the helicity of the outgoing electron is positive. The outgoing positrons, on the other hand, have positive helicities for the scalar operator and negative helicities for the vector operator. A measurement of these helicities can therefore be used to distinguish the two scenarios.

In the presence of the dipole and vector operators, which interfere at leading order in  $\hat{m}_e$ , the asymmetry does not simply range between the values in Table 2. For example, if only the coefficients  $C_{D,L}$  and  $C_{V,LL}^{ee}$  are non-zero, the asymmetry does not simply range between  $A_{\mu \rightarrow 3e}^P = -1$  and  $A_{\mu \rightarrow 3e}^P = 0.63$  in the limits  $|C_{D,L}| \ll |C_{V,LL}^{ee}|$  and  $|C_{D,L}| \gg |C_{V,LL}^{ee}|$ , respectively. Due to the interference between operators, the limits instead depend

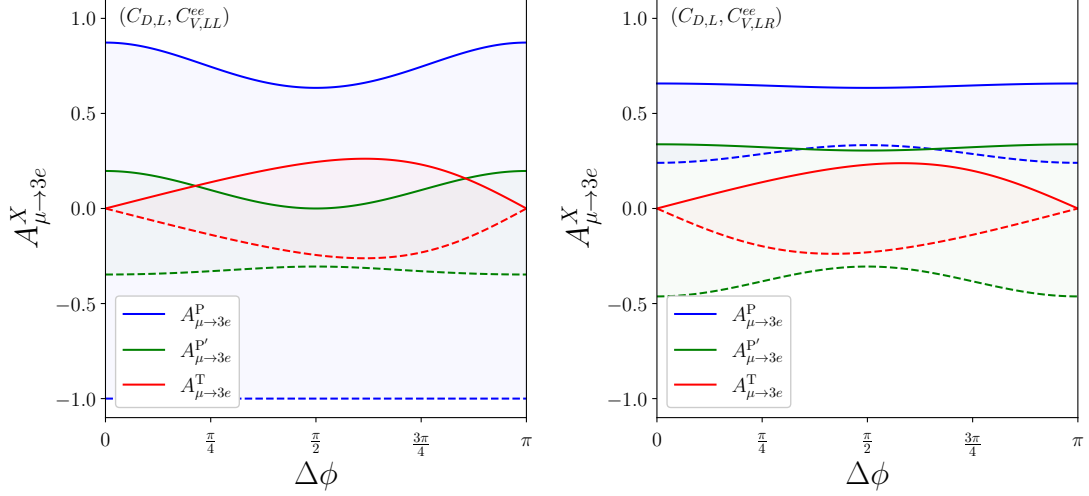


Figure 1: Ranges of the asymmetries  $A_{\mu \rightarrow 3e}^P$  (blue),  $A_{\mu \rightarrow 3e}^{P'}$  (green), and  $A_{\mu \rightarrow 3e}^T$  (red), with solid lines indicating the maximum asymmetries  $A_{\mu \rightarrow 3e}^{X+}$  and the dashed lines the minimum asymmetries  $A_{\mu \rightarrow 3e}^{X-}$ . In the left panel, only the coefficients  $C_{D,L}$  and  $C_{V,LL}^{ee}$  are taken to be non-zero, while in the right panel only  $C_{D,L}$  and  $C_{V,LR}^{ee}$  are considered. The ranges are shown as a function of the phase difference  $\Delta\phi$  between the coefficients.

on the relative phase  $\Delta\phi$  between the coefficients. For the coefficients  $C_{D,L}$  and  $C_{V,LL}^{ee}$ , the minimum and maximum values of  $A_{\mu \rightarrow 3e}^P$  depend on the phase as

$$A_{\mu \rightarrow 3e}^{P-} = -1, \quad A_{\mu \rightarrow 3e}^{P+} = 1 - \frac{3(57 \ln 2 - 47 + 4 \cos(2\Delta\phi))}{23 + 6 \cos(2\Delta\phi) + 12 \ln(4\hat{m}_e^2)}. \quad (19)$$

Correspondingly, the minimum and maximum values for  $A_{\mu \rightarrow 3e}^{P'}$  and  $A_{\mu \rightarrow 3e}^T$  are

$$A_{\mu \rightarrow 3e}^{P'\pm} = \frac{24(15 - 6 \cos(2\Delta\phi) \mp \sqrt{441 - 12(59 + 12 \ln(4\hat{m}_e^2)) \cos^2 \Delta\phi})}{35(23 + 6 \cos(2\Delta\phi) + 12 \ln(4\hat{m}_e^2))}, \quad (20)$$

$$A_{\mu \rightarrow 3e}^{T\pm} = \frac{\pm 144 \sin \Delta\phi}{35(6 \cos \Delta\phi + \sqrt{-51 - 36 \ln(4\hat{m}_e^2)})}. \quad (21)$$

In the left panel of Fig. 1, we depict the ranges of the asymmetries  $A_{\mu \rightarrow 3e}^P$  (blue),  $A_{\mu \rightarrow 3e}^{P'}$  (green), and  $A_{\mu \rightarrow 3e}^T$  (red) as a function of the relative phase  $\Delta\phi$  when only  $C_{D,L}$  and  $C_{V,LL}^{ee}$  are taken to be non-zero. The solid and dashed lines indicate the maximum and minimum asymmetries  $A_{\mu \rightarrow 3e}^{X+}$  and  $A_{\mu \rightarrow 3e}^{X-}$ , respectively. It can be seen that for  $\Delta\phi = 0$ , the P-odd asymmetry has the wider range of  $-1 \leq A_{\mu \rightarrow 3e}^P \leq 0.87$  compared to  $-1 \leq A_{\mu \rightarrow 3e}^{P'} \leq 0.63$  for  $\Delta\phi = \frac{\pi}{2}$ . In Fig. 1, right panel, we also show the ranges when  $C_{D,L}$  and  $C_{V,LR}^{ee}$  are taken to be non-zero.

If a future experiment does not observe  $\mu^+ \rightarrow e^+e^+e^-$  decay, this sets an upper limit on the branching ratio  $B_{\mu \rightarrow e\gamma}$  in Eq. (7) and therefore on each of the coefficients in Eq. (2) if the other coefficients are set to zero. A positive detection of  $\mu^+ \rightarrow e^+e^+e^-$  decay instead sets an allowed range for each coefficient. For example, an observed branching

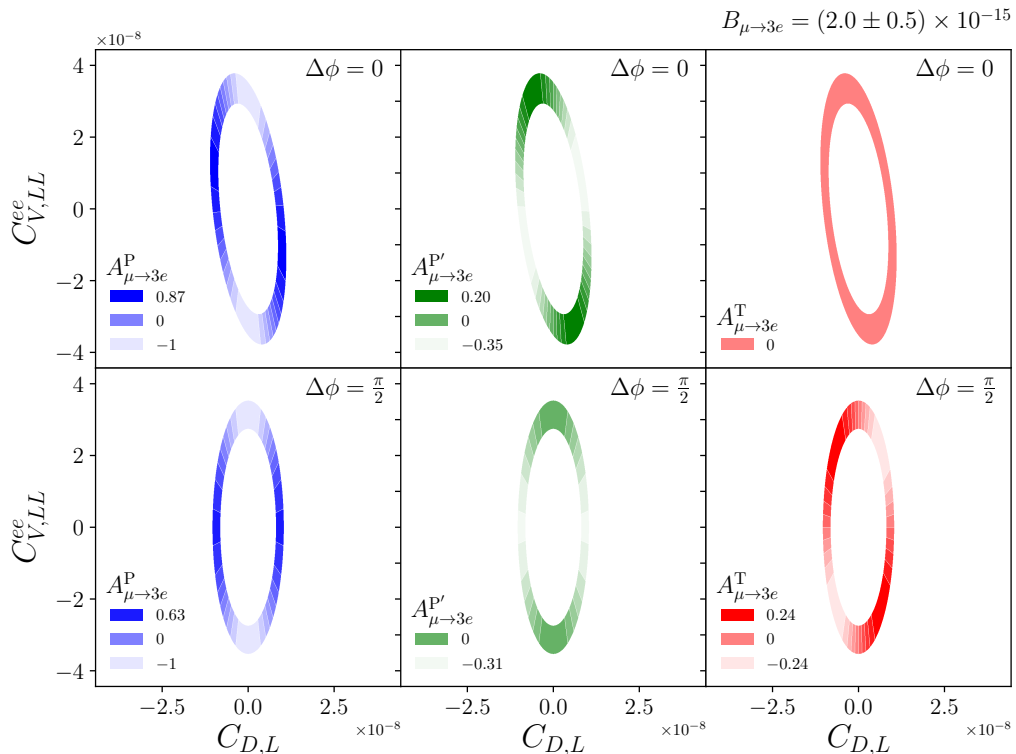


Figure 2: Assuming that the cLFV decay  $\mu^+ \rightarrow e^+e^+e^-$  is observed experimentally with a branching ratio of  $B_{\mu \rightarrow 3e} = (2.0 \pm 0.5) \times 10^{-15}$ , we depict the allowed regions in the  $(C_{D,L}, C_{V,LL}^{ee})$  parameter space for a relative phase difference between the coefficients of  $\Delta\phi = 0$  (top) and  $\Delta\phi = \frac{\pi}{2}$  (bottom). We also show the size of the asymmetries  $A_{\mu \rightarrow 3e}^P$  (left),  $A_{\mu \rightarrow 3e}^{P'}$  (middle), and  $A_{\mu \rightarrow 3e}^T$  (right). Measurements of these asymmetries can further constrain the parameter space, or indicate additional non-zero effective coefficients.

ratio of  $B_{\mu \rightarrow 3e} = (2.0 \pm 0.5) \times 10^{-15}$  constrains the dipole coefficients to lie in the range  $8.1 \times 10^{-9} \leq |C_{D,L(R)}| \leq 1.0 \times 10^{-8}$ . If two coefficients are allowed to be non-zero, the favoured region becomes an circle or ellipse in the parameter space of the coefficients. If the dipole and vector coefficients  $C_{D,L}$  and  $C_{V,LL}^{ee}$  (or  $C_{V,LR}^{ee}$ ) are taken to be non-zero, the alignment of the ellipse is controlled by the phase difference  $\Delta\phi$  between the coefficients. In Fig. 2, we plot the allowed regions in the  $(C_{D,L}, C_{V,LL}^{ee})$  plane if a future experiment measures  $B_{\mu \rightarrow 3e} = (2.0 \pm 0.5) \times 10^{-15}$ , for  $\Delta\phi = 0$  (top panels) and  $\Delta\phi = \frac{\pi}{2}$  (bottom panels). For  $\Delta\phi = 0$ , the real part of  $C_{D,L}C_{V,LL}^{ee*}$  in Eq. (7) is non-zero and therefore the ellipse is not aligned along the  $C_{D,L}$  and  $C_{V,LL}^{ee}$  axes. For  $\Delta\phi = \frac{\pi}{2}$ , the real part is indeed zero and the ellipse is aligned. In Fig. 2, we allow for negative values of the coefficients  $C_{D,L}$  and  $C_{V,LL}^{ee}$ . The allowed region for the phase difference  $\Delta\phi = \pi$  is therefore the mirror of the  $\Delta\phi = 0$  ellipse along either the  $C_{D,L}$  or  $C_{V,LL}^{ee}$  axis. In the left, centre and right panels of Fig. 2 we also show the magnitudes of the asymmetries  $A_{\mu \rightarrow 3e}^P$  (blue),  $A_{\mu \rightarrow 3e}^{P'}$  (green), and  $A_{\mu \rightarrow 3e}^T$  (red), respectively. The ranges of these asymmetries are consistent with the minimum and maximum values in Eqs. (19), (20) and (21).

We would finally like to note that a measurement of the process  $\mu^- e^- \rightarrow e^- e^-$  in

a muonic atom, first suggested in Ref. [66], can provide additional information on the effective coefficients of Eq. (2). Assuming a non-relativistic bound state for the muon, a 1S electron, a point nuclear charge and the plane wave approximation for the final-state electrons, one obtains an analytical result for the rate  $\Gamma(\mu^-e^- \rightarrow e^-e^-)$  with interference terms between the four-fermion operators [67]. The dependence of the rate on the dipole coefficients was studied separately in Ref. [68]; however, in principle there are also interference terms between the dipole and four-fermion operators. In a similar manner to the  $\mu^+ \rightarrow e^+e^+e^-$  process, the angular distribution of the outgoing electrons for a polarised muon can further identify the contribution of each operator [69]. In future, it is possible for Phase I of the COMET experiment to search for the clean signal of two back-to-back electrons with a total energy of the muon mass minus the muon binding energy [58]. A complete study of the complementarity of the cLFV processes in Table 1 (including measurements of angular distributions and helicities) is beyond the scope of this work.

## 4 Conclusions

In the present article, following a purely phenomenological approach, we have investigated the possibility to discriminate between different effective operators contributing at tree level to the amplitude of the polarised  $\mu^+ \rightarrow e^+e^+e^-$  decay by using data on the three angular observables – two P-odd and one T-odd asymmetries,  $A_{\mu \rightarrow 3e}^P$ ,  $A_{\mu \rightarrow 3e}^{P'}$  and  $A_{\mu \rightarrow 3e}^T$ , defined in Eqs. (15), (16) and (17). The consideration of these angular observables is particularly relevant as the next generation of experiments on  $\mu \leftrightarrow e$  cLFV processes are likely to use polarised muon beams. In particular, the high-intensity muon beams (HIMB) proposal at PSI aims to provide a flux of  $\mathcal{O}(10^9)$  longitudinally polarised muons per second to the Mu3e and MEG II experiments [51] on  $\mu^+ \rightarrow e^+e^+e^-$  and  $\mu^+ \rightarrow e^+\gamma$  decays, with the average  $\mu^+$  polarisation estimated to be approximately of 93%. The measurement of the P-odd asymmetry  $A_{\mu \rightarrow 3e}^P$  in the decay  $\mu^+ \rightarrow e^+e^+e^-$  requires the knowledge only of the direction of the outgoing electron and of the magnitude and the direction of the  $\mu^+$  polarisation. To determine the P-odd and T-odd asymmetries  $A_{\mu \rightarrow 3e}^{P'}$  and  $A_{\mu \rightarrow 3e}^T$ , it is also necessary to measure the directions of the outgoing positrons to identify the decay plane and the azimuthal angle  $\phi_\varepsilon$  between the  $\mu^+$  polarisation vector and the decay plane. The effective operators considered by us respect the CPT symmetry and thus an observation of a non-zero T-odd asymmetry would imply violation of the CP symmetry. This is only possible if at least two operators, which have different phases and whose interference term in the decay rate is not zero (i.e., is not strongly suppressed), generate the  $\mu^+ \rightarrow e^+e^+e^-$  decay.

The aim of our study was not to perform a comprehensive analysis of all operators that can induce the  $\mu^+ \rightarrow e^+e^+e^-$  decay, but to illustrate the effectiveness of the method on the example of the subset of eight commonly used effective operators that generate the decay at tree level, given in Eq. (2). This subset includes dimension-five left-handed ( $L$ ) and right-handed ( $R$ ) dipole operators and dimension-six four-fermion operators involving products of scalar and vector currents of different chiralities (left-left ( $LL$ ), right-right ( $RR$ ), left-right ( $LR$ ) and right-left ( $RL$ )). The only operators, among those considered

by us, that were found to have significant interference terms in the  $\mu^+ \rightarrow e^+e^+e^-$  decay rate at lowest order in  $m_e^2/m_\mu^2$ , are the dipole and vector operators. The interference between other operators was therefore neglected. Assuming the scale of NP to be around  $\Lambda_{\text{NP}} \sim 1$  TeV, one can neglect to a good approximation in the analysed P-odd and T-odd asymmetries the effects of the renormalisation group running of the considered operators above and below the electroweak scale.

It follows from the results of our study that if only one of the set of considered operators triggers the  $\mu^+ \rightarrow e^+e^+e^-$  decay, the measurement of the P-odd asymmetry  $A_{\mu \rightarrow 3e}^{\text{P}}$  can allow to discriminate between the dipole, scalar  $RR$  (scalar  $LL$ ), vector  $LL$  (vector  $RR$ ), vector  $LR$  and vector  $RL$  operators, while it will be impossible to distinguish between scalar  $RR$  (scalar  $LL$ ) and vector  $RR$  (vector  $LL$ ) operators (c.f. Table 2). With the measurement of  $A_{\mu \rightarrow 3e}^{\text{P}'}$  alone it may be possible to discriminate between the dipole, scalar or vector  $LL$  or  $RR$ , and vector  $LR$  or  $RL$  operators. At the same time, the difference between the values of  $A_{\mu \rightarrow 3e}^{\text{P}'}$  due to the dipole  $R$  (dipole  $L$ ) and vector  $RL$  (vector  $LR$ ) operators is very small (Table 2) and thus distinguishing between these operators requires an extremely high precision in the measurement of  $A_{\mu \rightarrow 3e}^{\text{P}'}$ .

In addition to the case of having just one operator responsible for the decay, we have derived predictions for the asymmetries of interest also in the cases when two operators are triggering the decay (Section 3). Some of these predictions are illustrated in Figs. 1 and 2. The observation of a non-zero T-odd asymmetry in the polarised  $\mu^+ \rightarrow e^+e^+e^-$  decay, for example, would imply that, within the considered set, the dipole and vector operators which have different phases are generating the decay.

It follows from the results of our study that if the  $\mu \leftrightarrow e$  cLFV processes are observed, the measurements of the angular distributions and of the corresponding P-odd and T-odd asymmetries in the  $\mu^+ \rightarrow e^+e^+e^-$  decay with polarised  $\mu^+$  would provide an effective additional method of identifying the beyond the SM new physics operators that trigger these processes.

## Acknowledgments

P. D. B. has received support from the European Union's Horizon 2020 research and innovation programme under the Marie Skłodowska-Curie grant agreement No 860881-HIDDeN. The work of S. T. P. was supported in part by the European Union's Horizon 2020 research and innovation programme under the Marie Skłodowska-Curie grant agreement No. 860881-HIDDeN, by the Italian INFN program on Theoretical Astroparticle Physics and by the World Premier International Research Center Initiative (WPI Initiative, MEXT), Japan.

# Appendix

## A Relevant Functions

The functions  $C_i(x_1, x_2)$  appearing in the differential branching ratio for the  $\mu^+ \rightarrow e^+ e^+ e^-$  decay in Eq. (3), where  $x_1 \equiv 2E_{k_1}/m_\mu$  and  $x_2 \equiv 2E_{k_2}/m_\mu$  and  $E_{k_1} \geq E_{k_2}$  are the outgoing positron energies, are of the form

$$\begin{aligned}
C_1(x_1, x_2) = & \left( \frac{|C_{S,LL}^{ee}|^2}{16} + |C_{V,LL}^{ee}|^2 \right) F_1(x_1, x_2) \\
& + |C_{V,LR}^{ee}|^2 F_2(x_1, x_2) + |eC_{D,L}|^2 F_3(x_1, x_2) \\
& + \text{Re}[eC_{D,L}C_{V,LL}^*] F_4(x_1, x_2) + \text{Re}[eC_{D,L}C_{V,LR}^*] F_5(x_1, x_2) \\
& + (L \leftrightarrow R), \tag{22}
\end{aligned}$$

$$\begin{aligned}
C_2(x_1, x_2) = & \left( \frac{|C_{S,LL}^{ee}|^2}{16} - |C_{V,LL}^{ee}|^2 \right) F_1(x_1, x_2) \\
& - |C_{V,LR}^{ee}|^2 G_2(x_1, x_2) + |eC_{D,L}|^2 G_3(x_1, x_2) \\
& - \text{Re}[eC_{D,L}C_{V,LL}^*] F_4(x_1, x_2) + \text{Re}[eC_{D,L}C_{V,LR}^*] F_5(x_1, x_2) \\
& - (L \leftrightarrow R), \tag{23}
\end{aligned}$$

$$\begin{aligned}
C_3(x_1, x_2) = & -|C_{V,LR}^{ee}|^2 H_2(x_1, x_2) + |eC_{D,L}|^2 H_3(x_1, x_2) \\
& + \text{Re}[eC_{D,L}C_{V,LL}^*] H_4(x_1, x_2) - \text{Re}[eC_{D,L}C_{V,LR}^*] H_5(x_1, x_2) \\
& - (L \leftrightarrow R), \tag{24}
\end{aligned}$$

$$\begin{aligned}
C_4(x_1, x_2) = & \text{Im}[eC_{D,L}C_{V,LL}^*] H_4(x_1, x_2) - \text{Im}[eC_{D,L}C_{V,LR}^*] H_5(x_1, x_2) \\
& + (L \leftrightarrow R). \tag{25}
\end{aligned}$$

Here, the functions  $F_i(x_1, x_2)$  are given by

$$\begin{aligned}
F_1(x_1, x_2) &= 8(2 - x_1 - x_2)(x_1 + x_2 - 1), \\
F_2(x_1, x_2) &= 2[x_1(1 - x_1) + x_2(1 - x_2)], \\
F_3(x_1, x_2) &= 8 \left[ \frac{2x_1^2 - 2x_1 + 1}{1 - x_2} + \frac{2x_2^2 - 2x_2 + 1}{1 - x_1} \right], \\
F_4(x_1, x_2) &= 32(x_1 + x_2 - 1), \\
F_5(x_1, x_2) &= 8(2 - x_1 - x_2), \tag{26}
\end{aligned}$$

the functions  $G_i(x_1, x_2)$  by

$$\begin{aligned}
G_2(x_1, x_2) &= 2 \frac{(x_1 + x_2)(x_1^2 + x_2^2) - 3(x_1 + x_2)^2 + 6(x_1 + x_2) - 4}{2 - x_1 - x_2}, \\
G_3(x_1, x_2) &= \frac{8}{(1 - x_1)(1 - x_2)(2 - x_1 - x_2)} \\
&\quad \times [2(x_1 + x_2)(x_1^3 + x_2^3) - 4(x_1 + x_2)(2x_1^2 + x_1x_2 + 2x_2^2) \\
&\quad + (19x_1^2 + 30x_1x_2 + 19x_2^2) - 12(2x_1 + 2x_2 - 1)], \tag{27}
\end{aligned}$$

and finally the  $H_i(x_1, x_2)$  functions by

$$\begin{aligned}
H_2(x_1, x_2) &= \frac{4(x_2 - x_1)}{2 - x_1 - x_2} \sqrt{(1 - x_1)(1 - x_2)(x_1 + x_2 - 1)}, \\
H_3(x_1, x_2) &= \frac{32(x_2 - x_1)(x_1 + x_2 - 1)}{2 - x_1 - x_2} \sqrt{\frac{x_1 + x_2 - 1}{(1 - x_1)(1 - x_2)}}, \\
H_4(x_1, x_2) &= 16(x_2 - x_1)(x_1 + x_2 - 1) \sqrt{\frac{x_1 + x_2 - 1}{(1 - x_1)(1 - x_2)}}, \\
H_5(x_1, x_2) &= 8(x_2 - x_1)(2 - x_1 - x_2) \sqrt{\frac{x_1 + x_2 - 1}{(1 - x_1)(1 - x_2)}}. \tag{28}
\end{aligned}$$

In these expressions we have neglected the electron mass  $m_e$ . These expressions are in agreement with those in Ref. [50].

It is straightforward to find the single differential branching ratio in the parameter  $x_1 = 2E_{k_1}/m_\mu$  as

$$\begin{aligned}
\frac{dB_{\mu \rightarrow 3e}}{dx_1} &= \left( \frac{|C_{S,LL}^{ee}|^2}{16} + |C_{V,LL}^{ee}|^2 \right) F'_1(x_1) \\
&\quad + |C_{V,LR}^{ee}|^2 F'_2(x_1) + |eC_{D,L}|^2 F'_3(x_1) \\
&\quad + \text{Re}[eC_{D,L}C_{V,LL}^*] F'_4(x_1) + \text{Re}[eC_{D,L}C_{V,LR}^*] F'_5(x_1) \\
&\quad + (L \leftrightarrow R), \tag{29}
\end{aligned}$$

where the  $F'_i(x_1)$  functions are computed as

$$F'_i(x_1) = 6 \int_{1-x_1}^{x_1} dx_2 F_i(x_1, x_2). \tag{30}$$

As mentioned in the main text, for the dipole operators one encounters a logarithmic divergence when neglecting the electron mass and performing the phase-space integral over  $x_1$ . The approach of Ref. [50] was to introduce a cut-off parameter  $\delta$  in the upper integration limit of  $x_1$ . However, the physical interpretation of  $\delta$  is unclear, and for numerical estimates it must be set arbitrarily to some value. In order to find the exact dependence of the total branching ratio  $B_{\mu \rightarrow 3e}$  and the P-odd asymmetry  $A_{\mu \rightarrow 3e}^P$  on the electron mass  $m_e$ , we instead express the differential branching ratio for  $\mu^+ \rightarrow e^+e^+e^-$  decay as a function of the kinematic variables  $s_1 = (p - k_1)^2 = m_\mu^2(1 - x_1) + m_e^2$  and  $s_2 = (p - k_2)^2 = m_\mu^2(1 - x_2) + m_e^2$ . We find (considering only the dipole operators)

$$\frac{dB_{\mu \rightarrow 3e}^{D,L(R)}}{ds_1 ds_2 d\Omega_\varepsilon} = \frac{3}{2\pi} \left[ \widehat{C}_1(s_1, s_2) + \widehat{C}_2(s_1, s_2) P \cos \theta_\varepsilon + \widehat{C}_3(s_1, s_2) P \sin \theta_\varepsilon \cos \phi_\varepsilon \right], \tag{31}$$

where the functions  $\widehat{C}_i(s_1, s_2)$  are given by

$$\widehat{C}_1(s_1, s_2) = \frac{8X}{m_\mu^6} \left[ -3m_e^2 + \frac{m_\mu^4 + 3m_e^4 - 2(m_\mu^2 + 3m_e^2)s_1 + 2s_1^2}{s_2} + \frac{2m_e^2(m_\mu^2 - m_e^2)^2}{s_2^2} + \frac{m_e^2(m_\mu^2 - m_e^2)(m_\mu^2 - 2m_e^2)}{s_1 s_2} + (s_1 \leftrightarrow s_2) \right], \quad (32)$$

$$\widehat{C}_2(s_1, s_2) = \frac{8Y}{m_\mu^8} \left[ -3m_\mu^4 - 2m_e^2 m_\mu^2 + 9m_e^4 + 3(m_\mu^2 - 2m_e^2)(s_1 + s_2) + s_1^2 + s_2^2 - \frac{2m_e^2 m_\mu^2 (m_\mu^2 - m_e^2) - (m_\mu^4 + 15m_e^4)s_1 + 2(m_\mu^2 + 5m_e^2)s_1^2 - 2s_1^3}{s_2} + \frac{2m_e^2(m_\mu^2 - m_e^2)^2(s_1 - 2m_e^2)}{s_2^2} + \frac{2m_e^2(m_\mu^2 - m_e^2)^2(m_\mu^2 - 2m_e^2)}{s_1 s_2} + (s_1 \leftrightarrow s_2) \right], \quad (33)$$

$$\widehat{C}_3(s_1, s_2) = \frac{16Z}{m_\mu^4} \left[ \frac{2m_\mu^2 + m_e^2 - 2s_1}{s_2} + \frac{2m_e^2(m_\mu^2 - m_e^2)}{s_2^2} - (s_1 \leftrightarrow s_2) \right], \quad (34)$$

with  $X \equiv |eC_{D,L}|^2 + |eC_{D,R}|^2$  and

$$Y \equiv \frac{1}{\lambda^{\frac{1}{2}}\left(\frac{m_e^2}{m_\mu^2}, \frac{s}{m_\mu^2}\right)} (|eC_{D,L}|^2 - |eC_{D,R}|^2), \quad Z \equiv \frac{Y}{m_\mu^3} \sqrt{ss_1 s_2 - m_e^2(m_\mu^2 - m_e^2)^2}, \quad (35)$$

where we have used  $\lambda(x, y) = (1 - x - y)^2 - 4xy$  and  $s = m_\mu^2 + 3m_e^2 - s_1 - s_2$ . Using the phase-space integration limits of  $s_1$  and  $s_2$  in Eqs. (4) and (5), respectively, we then obtain the total branching ratio as

$$\begin{aligned} B_{\mu \rightarrow 3e}^{D,L(R)} &= 6 \int_{4m_e^2}^{(m_\mu - m_e)^2} ds_1 \int_{s_1}^{s_2^+(s_1)} ds_2 \widehat{C}_1(s_1, s_2) \\ &= -\frac{8}{3} (|eC_{D,L}|^2 + |eC_{D,R}|^2) L_1(\hat{m}_e^2), \end{aligned} \quad (36)$$

where  $L_1(x) = 17 + 12 \ln 4x$  and we have only retained the terms at lowest order in an expansion in  $\hat{m}_e = \frac{m_e}{m_\mu}$ . The P-odd asymmetry is similarly found to be

$$\begin{aligned} A_{\mu \rightarrow 3e}^{PD,L(R)} &= \frac{6}{B_{\mu \rightarrow 3e}^{D,L(R)}} \int_{4m_e^2}^{(m_\mu - m_e)^2} ds_1 \int_{s_1}^{s_2^+(s_1)} ds_2 \widehat{C}_2(s_1, s_2) \\ &= \frac{1}{B_{\mu \rightarrow 3e}^{D,L(R)}} \left[ -\frac{8}{3} (|eC_{D,L}|^2 - |eC_{D,R}|^2) L_2(\hat{m}_e^2) \right], \end{aligned} \quad (37)$$

where  $L_2(x) = 170 - 171 \ln 2 + 12 \ln 4x$ .

## References

- [1] **KATRIN** Collaboration, M. Aker *et. al.*, *Improved Upper Limit on the Neutrino Mass from a Direct Kinematic Method by KATRIN*, Phys. Rev. Lett. **123** (2019), no. 22 221802, [arXiv:1909.06048].

- [2] M. Aker *et. al.*, *First direct neutrino-mass measurement with sub-eV sensitivity*, arXiv:2105.08533.
- [3] **Planck** Collaboration, N. Aghanim *et. al.*, *Planck 2018 results. VI. Cosmological parameters*, Astron. Astrophys. **641** (2020) A6, [arXiv:1807.06209]. [Erratum: Astron.Astrophys. 652, C4 (2021)].
- [4] **Particle Data Group** Collaboration, P. A. Zyla *et. al.*, *Review of Particle Physics*, PTEP **2020** (2020), no. 8 083C01. See Neutrinos in Cosmology review by J. Lesgourgues and L. Verde.
- [5] S. M. Bilenky and S. T. Petcov, *Massive Neutrinos and Neutrino Oscillations*, Rev. Mod. Phys. **59** (1987) 671. [Erratum: Rev.Mod.Phys. 61, 169 (1989), Erratum: Rev.Mod.Phys. 60, 575–575 (1988)].
- [6] S. T. Petcov, *The Processes  $\mu \rightarrow e + \gamma$ ,  $\mu \rightarrow e + \bar{e}$ ,  $\nu' \rightarrow \nu + \gamma$  in the Weinberg-Salam Model with Neutrino Mixing*, Sov. J. Nucl. Phys. **25** (1977) 340. [Erratum: Sov.J.Nucl.Phys. 25, 698 (1977), Erratum: Yad.Fiz. 25, 1336 (1977)].
- [7] S. M. Bilenky, S. T. Petcov, and B. Pontecorvo, *Lepton Mixing,  $\mu \rightarrow e + \gamma$  Decay and Neutrino Oscillations*, Phys. Lett. B **67** (1977) 309.
- [8] T. P. Cheng and L.-F. Li, *Nonconservation of Separate  $\mu$  - Lepton and  $e$  - Lepton Numbers in Gauge Theories with  $v+a$  Currents*, Phys. Rev. Lett. **38** (1977) 381.
- [9] **MEG** Collaboration, A. M. Baldini *et. al.*, *Search for the lepton flavour violating decay  $\mu^+ \rightarrow e^+ \gamma$  with the full dataset of the MEG experiment*, Eur. Phys. J. C **76** (2016), no. 8 434, [arXiv:1605.05081].
- [10] W. J. Marciano and A. I. Sanda, *Exotic Decays of the Muon and Heavy Leptons in Gauge Theories*, Phys. Lett. B **67** (1977) 303–305.
- [11] S. T. Petcov, *Heavy Neutral Lepton Mixing and  $\mu \rightarrow 3 e$  Decay*, Phys. Lett. B **68** (1977) 365–368.
- [12] A. Ilakovac and A. Pilaftsis, *Flavor violating charged lepton decays in seesaw-type models*, Nucl. Phys. B **437** (1995) 491, [hep-ph/9403398].
- [13] D. N. Dinh, A. Ibarra, E. Molinaro, and S. T. Petcov, *The  $\mu - e$  Conversion in Nuclei,  $\mu \rightarrow e \gamma$ ,  $\mu \rightarrow 3 e$  Decays and TeV Scale See-Saw Scenarios of Neutrino Mass Generation*, JHEP **08** (2012) 125, [arXiv:1205.4671]. [Erratum: JHEP 09, 023 (2013)].
- [14] R. Alonso, M. Dhen, M. B. Gavela, and T. Hambye, *Muon conversion to electron in nuclei in type-I seesaw models*, JHEP **01** (2013) 118, [arXiv:1209.2679].
- [15] D. N. Dinh and S. T. Petcov, *Lepton Flavor Violating  $\tau$  Decays in TeV Scale Type I See-Saw and Higgs Triplet Models*, JHEP **09** (2013) 086, [arXiv:1308.4311].

- [16] A. Abada and A. M. Teixeira, *Heavy neutral leptons and high-intensity observables*, Front. in Phys. **6** (2018) 142, [arXiv:1812.08062].
- [17] P. Minkowski,  $\mu \rightarrow e\gamma$  at a Rate of One Out of  $10^9$  Muon Decays?, Phys. Lett. B **67** (1977) 421–428.
- [18] T. Yanagida, *Horizontal Symmetry And Masses Of Neutrinos*, Conf.Proc. **C7902131** (1979) 95.
- [19] M. Gell-Mann, P. Ramond, and R. Slansky, *Complex Spinors and Unified Theories*, Conf. Proc. **C790927** (1979) 315–321, [arXiv:1306.4669].
- [20] S. Glashow, *Quarks and leptons*, . ed. M. Levy et al. (Plenum, New York), p. 707.
- [21] R. N. Mohapatra and G. Senjanović, *Neutrino masses and mixings in gauge models with spontaneous parity violation*, Phys. Rev. **D23** (1981) 165.
- [22] W. Konetschny and W. Kummer, *Nonconservation of Total Lepton Number with Scalar Bosons*, Phys. Lett. B **70** (1977) 433–435.
- [23] M. Magg and C. Wetterich, *Neutrino Mass Problem and Gauge Hierarchy*, Phys. Lett. B **94** (1980) 61–64.
- [24] T. P. Cheng and L.-F. Li, *Neutrino Masses, Mixings and Oscillations in  $SU(2) \times U(1)$  Models of Electroweak Interactions*, Phys. Rev. D **22** (1980) 2860.
- [25] R. Foot, H. Lew, X. G. He, and G. C. Joshi, *Seesaw Neutrino Masses Induced by a Triplet of Leptons*, Z. Phys. C **44** (1989) 441.
- [26] A. Abada, C. Biggio, F. Bonnet, M. B. Gavela, and T. Hambye,  $\mu \rightarrow e \gamma$  and  $\tau \rightarrow l \gamma$  decays in the fermion triplet seesaw model, Phys. Rev. D **78** (2008) 033007, [arXiv:0803.0481].
- [27] A. Zee, *A Theory of Lepton Number Violation, Neutrino Majorana Mass, and Oscillation*, Phys. Lett. B **93** (1980) 389. [Erratum: Phys.Lett.B 95, 461 (1980)].
- [28] S. T. Petcov, *Remarks on the Zee Model of Neutrino Mixing ( $\mu \rightarrow e \gamma$ , Heavy Neutrino  $\rightarrow$  Light Neutrino  $\gamma$ , etc.)*, Phys. Lett. B **115** (1982) 401–406.
- [29] K. S. Babu, *Model of 'Calculable' Majorana Neutrino Masses*, Phys. Lett. B **203** (1988) 132–136.
- [30] E. Ma, *Verifiable radiative seesaw mechanism of neutrino mass and dark matter*, Phys. Rev. D **73** (2006) 077301, [hep-ph/0601225].
- [31] Y. Cai, J. Herrero-García, M. A. Schmidt, A. Vicente, and R. R. Volkas, *From the trees to the forest: a review of radiative neutrino mass models*, Front. in Phys. **5** (2017) 63, [arXiv:1706.08524].

- [32] V. Cirigliano, B. Grinstein, G. Isidori, and M. B. Wise, *Minimal flavor violation in the lepton sector*, Nucl. Phys. B **728** (2005) 121–134, [[hep-ph/0507001](#)].
- [33] S. Davidson and F. Palorini, *Various definitions of Minimal Flavour Violation for Leptons*, Phys. Lett. B **642** (2006) 72–80, [[hep-ph/0607329](#)].
- [34] M. B. Gavela, T. Hambye, D. Hernandez, and P. Hernandez, *Minimal Flavour Seesaw Models*, JHEP **09** (2009) 038, [[arXiv:0906.1461](#)].
- [35] R. Alonso, G. Isidori, L. Merlo, L. A. Munoz, and E. Nardi, *Minimal flavour violation extensions of the seesaw*, JHEP **06** (2011) 037, [[arXiv:1103.5461](#)].
- [36] D. N. Dinh, L. Merlo, S. T. Petcov, and R. Vega-Álvarez, *Revisiting Minimal Lepton Flavour Violation in the Light of Leptonic CP Violation*, JHEP **07** (2017) 089, [[arXiv:1705.09284](#)].
- [37] L. Calibbi and G. Signorelli, *Charged Lepton Flavour Violation: An Experimental and Theoretical Introduction*, Riv. Nuovo Cim. **41** (2018), no. 2 71–174, [[arXiv:1709.00294](#)].
- [38] F. Gabbiani and A. Masiero, *FCNC in Generalized Supersymmetric Theories*, Nucl. Phys. B **322** (1989) 235–254.
- [39] R. Barbieri, L. J. Hall, and A. Strumia, *Violations of lepton flavor and CP in supersymmetric unified theories*, Nucl. Phys. B **445** (1995) 219–251, [[hep-ph/9501334](#)].
- [40] J. Hisano, T. Moroi, K. Tobe, and M. Yamaguchi, *Lepton flavor violation via right-handed neutrino Yukawa couplings in supersymmetric standard model*, Phys. Rev. D **53** (1996) 2442–2459, [[hep-ph/9510309](#)].
- [41] J. Hisano and D. Nomura, *Solar and atmospheric neutrino oscillations and lepton flavor violation in supersymmetric models with the right-handed neutrinos*, Phys. Rev. D **59** (1999) 116005, [[hep-ph/9810479](#)].
- [42] J. A. Casas and A. Ibarra, *Oscillating neutrinos and  $\mu \rightarrow e, \gamma$* , Nucl. Phys. B **618** (2001) 171–204, [[hep-ph/0103065](#)].
- [43] F. Deppisch and J. W. F. Valle, *Enhanced lepton flavor violation in the supersymmetric inverse seesaw model*, Phys. Rev. D **72** (2005) 036001, [[hep-ph/0406040](#)].
- [44] E. Arganda, M. J. Herrero, and A. M. Teixeira,  *$\mu$ - $e$  conversion in nuclei within the CMSSM seesaw: Universality versus non-universality*, JHEP **10** (2007) 104, [[arXiv:0707.2955](#)].
- [45] G. Altarelli, F. Feruglio, L. Merlo, and E. Stamou, *Discrete Flavour Groups,  $\theta_{13}$  and Lepton Flavour Violation*, JHEP **08** (2012) 021, [[arXiv:1205.4670](#)].

- [46] G. Bambhaniya, P. S. B. Dev, S. Goswami, and M. Mitra, *The Scalar Triplet Contribution to Lepton Flavour Violation and Neutrinoless Double Beta Decay in Left-Right Symmetric Model*, JHEP **04** (2016) 046, [arXiv:1512.00440].
- [47] S. Davidson, *Completeness and complementarity for  $\mu \rightarrow e\gamma$ ,  $\mu \rightarrow e\bar{e}e$  and  $\mu A \rightarrow eA$* , JHEP **02** (2021) 172, [arXiv:2010.00317].
- [48] V. Cirigliano, S. Davidson, and Y. Kuno, *Spin-dependent  $\mu \rightarrow e$  conversion*, Phys. Lett. B **771** (2017) 242–246, [arXiv:1703.02057].
- [49] S. Davidson, Y. Kuno, and M. Yamanaka, *Selecting  $\mu \rightarrow e$  conversion targets to distinguish lepton flavour-changing operators*, Phys. Lett. B **790** (2019) 380–388, [arXiv:1810.01884].
- [50] Y. Okada, K.-i. Okumura, and Y. Shimizu,  *$\mu \rightarrow e$  gamma and  $\mu \rightarrow 3e$  processes with polarized muons and supersymmetric grand unified theories*, Phys. Rev. D **61** (2000) 094001, [hep-ph/9906446].
- [51] M. Aiba *et. al.*, *Science Case for the new High-Intensity Muon Beams HIMB at PSI*, arXiv:2111.05788.
- [52] **MEG II** Collaboration, A. M. Baldini *et. al.*, *The design of the MEG II experiment*, Eur. Phys. J. C **78** (2018), no. 5 380, [arXiv:1801.04688].
- [53] R. D. Bolton *et. al.*, *Search for Rare Muon Decays with the Crystal Box Detector*, Phys. Rev. D **38** (1988) 2077.
- [54] **SINDRUM** Collaboration, U. Bellgardt *et. al.*, *Search for the Decay  $\mu^+ \rightarrow e^+ e^+ e^-$* , Nucl. Phys. B **299** (1988) 1–6.
- [55] **Mu3e** Collaboration, K. Arndt *et. al.*, *Technical design of the phase I Mu3e experiment*, Nucl. Instrum. Meth. A **1014** (2021) 165679, [arXiv:2009.11690].
- [56] A. Badertscher *et. al.*, *New Upper Limits for Muon - Electron Conversion in Sulfur*, Lett. Nuovo Cim. **28** (1980) 401–408.
- [57] **Mu2e** Collaboration, L. Bartoszek *et. al.*, *Mu2e Technical Design Report*, arXiv:1501.05241.
- [58] **COMET** Collaboration, R. Abramishvili *et. al.*, *COMET Phase-I Technical Design Report*, PTEP **2020** (2020), no. 3 033C01, [arXiv:1812.09018].
- [59] **SINDRUM II** Collaboration, C. Dohmen *et. al.*, *Test of lepton flavor conservation in  $\mu \rightarrow e$  conversion on titanium*, Phys. Lett. B **317** (1993) 631–636.
- [60] Y. Kuno *et. al.*, *An Experimental Search for a  $\mu N \rightarrow eN$  Conversion at Sensitivity of the Order of  $10^{-18}$  with a Highly Intense Muon Source: PRISM*, unpublished (2006).

- [61] **SINDRUM II** Collaboration, W. H. Bertl *et. al.*, *A Search for muon to electron conversion in muonic gold*, Eur. Phys. J. C **47** (2006) 337–346.
- [62] **SINDRUM II** Collaboration, W. Honecker *et. al.*, *Improved limit on the branching ratio of  $\mu \rightarrow e$  conversion on lead*, Phys. Rev. Lett. **76** (1996) 200–203.
- [63] Y. Kuno and Y. Okada, *Muon decay and physics beyond the standard model*, Rev. Mod. Phys. **73** (2001) 151–202, [[hep-ph/9909265](#)].
- [64] Y. Okada, K.-i. Okumura, and Y. Shimizu, *CP violation in the  $\mu \rightarrow 3 e$  process and supersymmetric grand unified theory*, Phys. Rev. D **58** (1998) 051901, [[hep-ph/9708446](#)].
- [65] A. Ilakovac, A. Pilaftsis, and L. Popov, *Charged lepton flavor violation in supersymmetric low-scale seesaw models*, Phys. Rev. D **87** (2013), no. 5 053014, [[arXiv:1212.5939](#)].
- [66] M. Koike, Y. Kuno, J. Sato, and M. Yamanaka, *A new idea to search for charged lepton flavor violation using a muonic atom*, Phys. Rev. Lett. **105** (2010) 121601, [[arXiv:1003.1578](#)].
- [67] Y. Uesaka, Y. Kuno, J. Sato, T. Sato, and M. Yamanaka, *Improved analyses for  $\mu^- e^- \rightarrow e^- e^-$  in muonic atoms by contact interactions*, Phys. Rev. D **93** (2016), no. 7 076006, [[arXiv:1603.01522](#)].
- [68] Y. Uesaka, Y. Kuno, J. Sato, T. Sato, and M. Yamanaka, *Improved analysis for  $\mu^- e^- \rightarrow e^- e^-$  in muonic atoms by photonic interaction*, Phys. Rev. D **97** (2018), no. 1 015017, [[arXiv:1711.08979](#)].
- [69] Y. Kuno, J. Sato, T. Sato, Y. Uesaka, and M. Yamanaka, *Momentum distribution of the electron pair from the charged lepton flavor violating process  $\mu^- e^- \rightarrow e^- e^-$  in muonic atoms with a polarized muon*, Phys. Rev. D **100** (2019), no. 7 075012, [[arXiv:1908.11653](#)].